



# Manufacturing Water-Based Low-Tortuosity Electrodes for Fast-Charge through Pattern Integrated Stamping

Haoze Ren , Ying Wang, Daxian Cao, William Gedney , Tongtai Ji, Xiao Sun, and Hongli Zhu\*


**Achieving high energy density and fast charging of lithium-ion batteries can accelerate the promotion of electric vehicles. However, the increased mass loading causes poor charge transfer, impedes the electrochemical reaction kinetics, and limits the battery charging rate. Herein, this work demonstrated a novel pattern integrated stamping process for creating channels in the electrode, which benefits ion transport and increases the rate performance of the electrode. Meanwhile, the pressure applied during the stamping process improved the contact between electrode and current collector and also enhanced the mechanical stability of the electrode. Compared to the conventional bar-coated electrode with the same thickness of 155  $\mu\text{m}$  (delivered a discharge capacity of 16  $\text{mAh g}^{-1}$  at the rate of 3 C), the stamped low-tortuosity  $\text{LiFePO}_4$  electrode delivered 101  $\text{mAh g}^{-1}$  capacity. Additionally, water was employed as a solvent in this study. Owing to its eco-friendliness, high scalability, and minimal waste generation, this novel stamping technique inspire a new method for the industrial-level efficient roll to roll fabrication of fast-charge electrodes.**

## 1. Introduction

The development of lithium-ion batteries (LIBs) with high energy densities and long cycle lives is crucial for enlarging the applied range of electric vehicles (EVs).<sup>[1–3]</sup> In addition, fast-charging LIBs with high mass loading are essential for meeting the growing energy requirements of EVs.<sup>[4]</sup> Currently, the factors that limit the LIBs charging capacities at high rate are the low mass-transfer ability of the electrolyte<sup>[5]</sup> and the slow ion transport in conventional electrodes, which hinder the overall ion diffusion rate.<sup>[6]</sup> During fast charging, lithium ions are depleted at a certain depth from the electrode surface, beyond which the active material cannot be utilized. Therefore, electrodes with low mass loading are preferred for fast charging applications.<sup>[7]</sup> However, low mass loading leads to a reduced areal energy density, which impedes improvement of the mile range of EVs.<sup>[8]</sup> Current state-of-the-art research focuses primarily on electrolyte engineering and electrode structure modification to solve this problem.<sup>[9–12]</sup>

Low-tortuosity electrodes accelerate the diffusion of lithium ions and provide the shortest path for ion transport. Additionally, the porous

H. Ren, Y. Wang, Dr. D. Cao, W. Gedney, T. Ji, X. Sun, Prof. H. Zhu  
Department of Mechanical and Industrial Engineering, Northeastern University, Boston MA 02115, USA  
E-mail: h.zhu@neu.edu

 The ORCID identification number(s) for the author(s) of this article can be found under <https://doi.org/10.1002/eem2.12584>.

DOI: 10.1002/eem2.12584

electrode surface enhances electrolyte absorption and improves the mass transfer of reactants.<sup>[13–15]</sup> Several methods have been reported recently for the fabrication of low-tortuosity electrodes, such as magnetic alignment,<sup>[16]</sup> laser perforation,<sup>[17]</sup> 3D printing,<sup>[18]</sup> and the utilization of organic structures, such as wood.<sup>[19]</sup> Despite their better rate performance and stability compared to bar-coated electrodes, the fabrication of low-tortuosity electrodes using the aforementioned methods is time-consuming and expensive. For example, the magnetic alignment method introduces magnetic impurities into the electrode, which requires additional processing steps for their removal. The high cost and complexity of the fabrication process, together with its low efficiency, hindered its adoption for industrial production.

In contrast to the aforementioned methods, the simple and adaptable stamping method described here is capable of producing low-cost low-tortuosity electrodes. This technology

enables the direct transfer of the electrode slurry onto the current collector by exploiting the adhesion between the two materials and the fluidity of the slurry. When stamping slurry with high flowability, the pattern created on the electrode can be damaged after the stamp separation owing to the slurry flow. By taking advantage of the stronger adhesion between the electrode slurry and current collector, the slurry and stamp can be separated without material loss, leaving the patterned electrode intact. Furthermore, owing to the simplicity of the stamping method, the fabrication time is similar to that of the conventional coating techniques. In addition, the applied pressure during the stamping process simulates the normal force during the calendaring treatment in the traditional fabrication processes. The applied pressure enhances the contact between the particles in the electrode material, thus improving the electrical conductivity and rate performance. It also optimizes the contact between the electrode and current collector, ensuring better charge transfer, mechanical and structural stability, and improved cycling life and rate performance of the battery.<sup>[20,21]</sup>

Here, we employed a simple stamping process to fabricate low-tortuosity electrodes. We then evaluated the effect of the electrode structure on the fast-charging properties of the electrode. Compared to conventional bar-coated electrodes, stamped electrodes exhibit outstanding improvements in electrolyte wettability, charge-discharge capacity retention at high currents, and cycling performance. These advantages can be attributed to the unique electrode structure consisting of uniformly arranged microchannels and the tight packing of the electrode

material caused by the pressure applied during the stamping process. This work provides a new route for the design and fabrication of low-tortuosity fast-charging electrodes that can be implemented in conventional roll-to-roll (R2R) manufacturing.

## 2. Results and Discussions

For conventional electrodes, random and tight stacking of the electrode material particles results in a circuitous pore structure (Figure 1a). The resulting high-tortuosity path hinders electrolyte penetration into the electrode and significantly increases the ion-transfer distance. Figure 1b

shows that a low-tortuosity electrode structure can improve the electrode accessibility to the electrolyte and shorten the ion-transfer path during the battery charge and discharge. This, in turn, can accelerate the transport of lithium ions between the electrolyte and electrode. Figure 1c shows the fabrication process of the stamped low-tortuosity electrode. The surface pattern of the stamp consisted of hexagonally packed cylinders of diameter 100  $\mu\text{m}$  separated by 100  $\mu\text{m}$  gaps, as shown in Figure S1, Supporting Information. After adding the electrode slurry to the stamp surface, the loaded stamp was pressed onto the current collector. A normal force was applied at the back of the stamp to fully compress the slurry and ensure conformal contact with the collector. To ensure a complete separation, the stamp was kept steady and dried

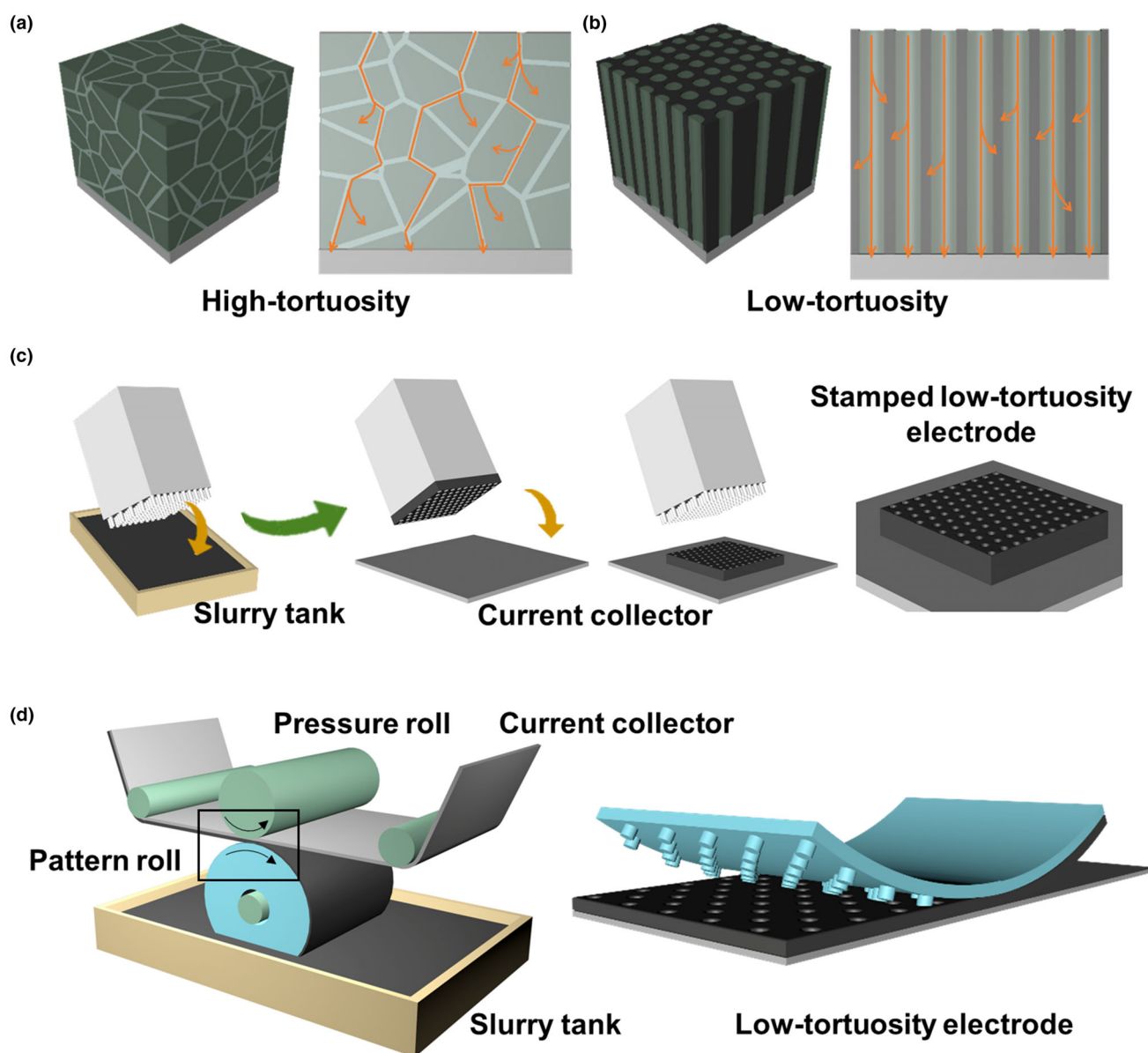


**Figure 1.** Schematic representation of the low-tortuosity and bar-coated high-tortuosity electrode structures, and the proposed stamping method. a) Conventional bar-coated electrode structure. b) Stamped low-tortuosity electrode structure. c) Fabrication of low-tortuosity electrode using the stamping method. d) Scaling up of the stamping method for industrial R2R manufacturing.

for 30 s with a vertical force applied. After that, a small gap formed between the slurry surface and the pattern, assisting the ink release from the stamp.

This stamping technique can be scaled up and integrated into existing R2R processes for the industrial manufacturing of low-tortuosity electrodes. The schematic of the R2R stamping, shown in Figure 1d, highlights the two main units: pattern roll and pressure roll. In industrial R2R fabrication, the pattern roll transfers the slurry from a tank to the current collector surface. The pressure roll exerts pressure on the opposite side of the current collector, ensuring a complete transfer of the electrode slurry and control of the electrode thickness.

Optimizing the slurry composition is crucial for ensuring successful stamping of low-tortuosity electrodes. In this study, we compared the stamping performance of slurries with a solid content of 40 and 65 wt.%. Figure S2, Supporting Information shows photographs of the two different as-prepared slurries. The high concentration slurry exhibits higher viscosity than 40 wt.% slurry, and its outstanding plasticity is suitable for stamped technology.<sup>[22]</sup> Lithium iron phosphate (LiFePO<sub>4</sub>, LFP), carbon black (CB, Super P), and a mixture of carboxymethyl cellulose sodium salt (CMC) and styrene-butadiene rubber (SBR) were used as the active material, conductive additive, and electrode binder, respectively (LiFePO<sub>4</sub>:Super P:CMC/SBR = 87:10:3) (Figure S3, Supporting Information). Owing to the better stability in water than lithium nickel manganese cobalt oxides, LFP is an excellent cathode material to adopt aqueous-based electrode processing.<sup>[23]</sup> The prepared 40 and 65 wt.% slurries were placed into vials and stored vertically until they had completely settled. The vials were then rotated at 180° horizontally and observed to estimate the slurry viscosity. The slurry with 65 wt.% solid content was highly viscous and firmly stuck to the bottom of the vial. The viscosity of the slurry with 40 wt.% solid content appeared to be too low and unsuitable for stamping.

Both slurries were stamped onto a current collector, and the resulting morphologies are shown in Figure S4, Supporting Information. The electrode structure fabricated using low-solid-content slurry appeared as a tree branch, which was caused by the tendency of the slurry to stick to the stamp surface during the separation. The electrode fabricated using high-solid-content slurry exhibited a well-defined pore structure corresponding to the stamp pattern. High-speed imaging data (Figure S5, Supporting Information) enabled the study of the slurry behavior during the stamping process. In the case of the high-solid-content slurry, the stamp separated easily from the electrode without any slurry residue. When stamping using the low-solid-content slurry, a curved slurry bridge was formed between the stamp and current collector, as shown in Figure S5d, Supporting Information, which prevented the clean separation of the two parts.

The stamped electrode exhibited better structural stability even at larger thickness compared to bar-coated electrodes, which can improve the cycling stability of electrodes with higher mass loading. Figure 2a,b show stamped and bar-coated electrodes, respectively, of thickness 150, 200, and 250 μm. At thickness of 150 μm, both types of electrodes remained intact and in close contact with the current collector. As the thickness of the bar-coated electrode increased to 200 μm, cracks began to appear on the electrode surface. Further increase of the thickness to 250 μm resulted in prominent cracks and flaking of the electrode material. Figure S6, Supporting Information shows the dried bar-coated electrodes of thicknesses 200 and 250 μm before punching; the electrodes had developed visible cracks when they were drying. In contrast, there were no observable cracks in the 200 μm-thick stamped electrode and only a minor crack in the 250 μm-thick electrode. The applied pressure

during the stamping process enhanced the contact between the electrode particles, resulting in better adhesion between the electrode and current collector and improved integrity of the electrode at larger thickness. In addition, the channels on the stamped electrode surface also facilitated water evaporation and provided additional space to accommodate electrode volume deformation during the drying process, thus preserving the structural integrity of the stamped electrode.

Improving the electrolyte wettability of the electrode is of particular importance for the development of fast-charging batteries. Electrodes with poor wettability produce unstable solid electrolyte interface film, which hinders the redox reaction and degrades the performance of the electrode. Due to the rapid electrolyte absorption by the electrode, it was difficult to accurately measure the contact angle between the electrode and electrolyte. Hence, we measured the speed of electrolyte absorption by the electrode to evaluate the electrolyte wettability of the electrode. As shown in Figure 2c, the stamped electrode required 3 s to fully absorb 2 μL of the electrolyte. In contrast, bar-coated electrode took 7 s to completely absorb the electrolyte droplet (Figure 2d). The observed faster electrolyte absorption by the stamped electrode indicates better electrolyte wettability compared to the bar-coated electrode due to the stamped multichannels. Figure S7a,b, Supporting Information show the water contact angles of the stamped and bar-coated electrodes, respectively, 1 s after the water droplet deposition. The contact angle of the stamped electrode was 35°, which is smaller than the contact angle of 43° exhibited by the bar-coated electrode. For the electrode hydrophilic surfaces, the increased roughness and porosity of the surface result in a smaller interfacial water contact angle.<sup>[24]</sup> In this study, the smaller water contact angle of the stamped electrode can be attributed to its higher surface roughness.

The scanning electron microscopy (SEM) images in Figure 3 show the microstructure of the stamped and bar-coated electrodes. Figure 3a, b represent top-view SEM images of the stamped low-tortuosity electrode, which exhibits a rough surface decorated with micrometer-sized channels arranged in a “honeycomb” pattern, consistent with the stamp pattern. The microchannels had a tapered shape with a top diameter of 120 μm, as shown in the cross-sectional SEM images (Figure 3d,e). The channel depth was 71 μm, which is less than the electrode thickness, because of the material buildup during the drying process and uneven pattern surface. Figure 3g,h represent the top-view and cross-sectional images of the bar-coated electrode, respectively. The electrode surface appeared rough with tightly packed electrode particles, suggesting that the highly tortuous paths formed in the electrode material are the only available ion transport route. To investigate the effect of the stamping method on the particle distribution in the electrode material, high-magnification SEM images were acquired at the channel edge of the stamped electrode (Figure 3c,f) and compared with the images of the bar-coated electrode (Figure 3i). The LFP and CB particles were distributed similarly in both electrodes, indicating that the stamping process had no observable effect on the electrode components distribution and interconnection of LFP and CB.

To study the battery interface stability, two batteries assembled using bar-coated-T (same thickness as stamped electrode) and stamped electrodes were investigated by electrochemical impedance spectroscopy (EIS). Figure 4a shows Nyquist plots of the two electrodes. The semicircular patterns in the high-frequency region are clear, and the diameter of the semicircles represents the charge resistance of the two electrodes. The EIS results show smaller resistance of the stamped electrode in the high- and medium-frequency regions compared to that of the bar-coated-T electrode, confirming the improved charge transfer



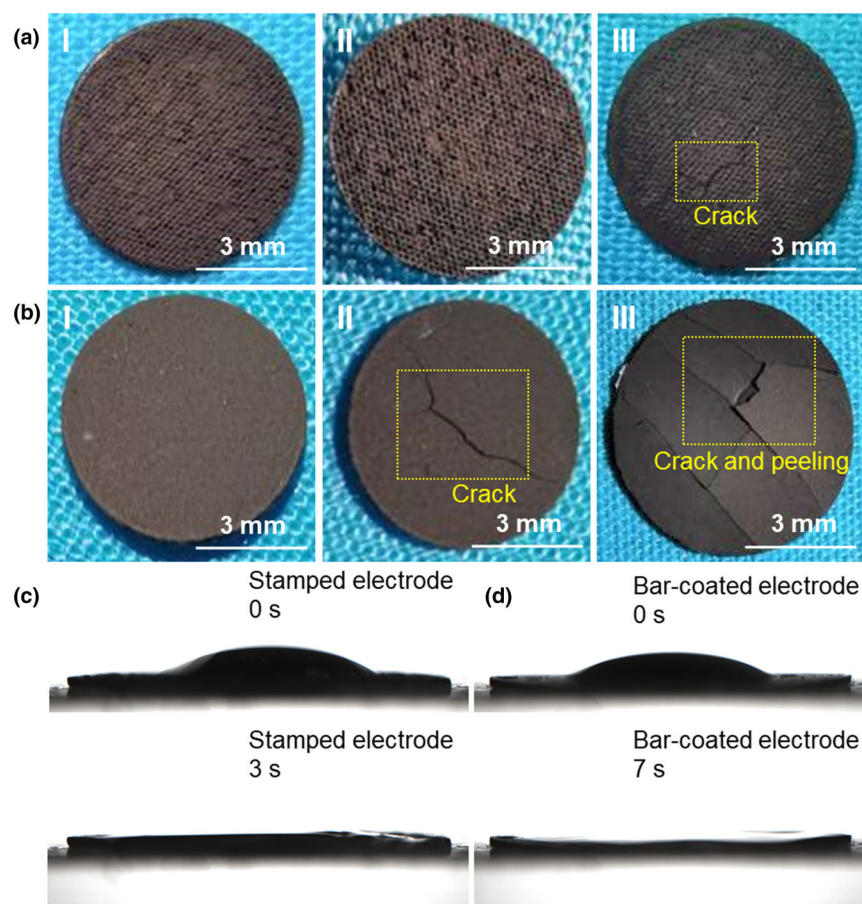


**Figure 2.** Physical property characterization of the stamped and bar-coated electrodes. a) Photographs of stamped electrodes with thickness of I) 150  $\mu\text{m}$ , II) 200  $\mu\text{m}$ , and III) 250  $\mu\text{m}$ . b) Photographs of bar-coated electrodes with thickness of I) 150  $\mu\text{m}$ , II) 200  $\mu\text{m}$ , and III) 250  $\mu\text{m}$ . c) Electrolyte absorption time of the stamped electrode. d) Electrolyte absorption time of the bar-coated electrode.

kinetics of the stamped electrode. The enhanced performance can be attributed to the lower tortuosity of the stamped structure, which provides a larger electrode/electrolyte contact area and improves the charge transfer kinetics at the electrode interface. To investigate the effect of the electrode thickness on the electrode interface resistance, we performed EIS measurements on stamped electrodes of different thickness. The diameters of the high-frequency semicircles in the Nyquist plots, shown in Figure 4b, gradually increased with the increase in the electrode thickness. For thick electrodes, the ion-transfer rate is the main factor limiting the charge transfer process.<sup>[25]</sup> As the thickness increased, the mass transfer rate of the electrode decreased, and its charge transfer resistance increased. Figure 4c shows the cyclic voltammetry (CV) curves of the stamped and bar-coated-T electrodes. The stamped electrode showed a narrower spread of the redox peaks than the bar-coated-T electrode, indicating better electrochemical kinetic behavior in the stamped electrode.

The charge and discharge profiles of the stamped and bar-coated-T electrodes at current rates of 0.1, 2, and 3 C are shown in Figure 4d–f. Both electrodes showed a flatter voltage plateau around 3.5 V at 0.1 C. As the current rate increased, the voltage plateau of the stamped electrode shifted slightly to approximately 3.6 V at 3 C, whereas the voltage plateau of the bar-coated-T electrode increased dramatically. The potential of the two batteries was compared at 50% of the state of

charge and depth of discharge to evaluate the electrochemical reaction kinetics. At charge–discharge current rates of 2 and 3 C which displayed in Figure 4e,f, the overpotential of the bar-coated-T electrode battery was significantly higher, confirming the lower reaction kinetics and worse rate performance of the bar-coated-T electrode battery.<sup>[26]</sup> Another bar-coated electrode was assembled as control sample, keeping the same active material areal mass loading (named as bar-coated-M) as stamped electrode. Figure 4g,h show the measured charge and discharge capacities of three electrodes. At a rate of 0.1 C, the average capacity of the stamped electrode was 172  $\text{mAh g}^{-1}$ , with a charge capacity of 101  $\text{mAh g}^{-1}$  at a current rate of 3 C. Notably, when the current rate increased from 0.1 to 1 C, we observed no apparent decrease in the capacity, which demonstrates the excellent rate performance of the stamped electrode. Under the same conditions, the average charge capacity of the bar-coated-T electrode was 160, 151, 140, 107, and 16  $\text{mAh g}^{-1}$  at current rates of 0.1, 0.5, 1, 2, and 3 C, respectively. Benefiting from its relatively lower thickness than other two electrodes, the bar-coated-M electrode showed a higher average charge capacity of 0.1 C (188  $\text{mAh g}^{-1}$ ). The rate performance of the bar-coated-M electrode was observed from the decreased capacities of 134 and 54  $\text{mAh g}^{-1}$  at the increased rate of 1 and 3 C, respectively. Upon reducing the current rate to 0.1 C, the capacity of three electrodes recovered to the initial value. The areal capacities are displayed

in Figure 4i. A large ratio of the stamped electrode area capacity was retained at the wide applicable relevant current rates (>94% at 0.5 C, >86% at 1 C, >72% at 2 C, and >58% at 3 C). Despite the capacity decrease at high rates, the stamped electrode consistently outperformed the bar-coated-M electrode. Our results demonstrate that the stamped low-tortuosity electrode structure exhibits better fast-charging performance compared to the bar-coated electrode. The improved rate performance of the stamped electrode can be attributed to the uniformly aligned channels, which reduce the lithium-ion transport distance between the cathode and the separator, thus increasing the ionic transport efficiency.

The long-term cycling performance of both electrodes was evaluated at a current rate of 1 C. As shown in Figure 5a, both electrodes maintained approximately 98.7% Coulombic efficiency over 50 cycles. The stamped electrode battery exhibited superior stability compared to the bar-coated-T electrode battery. After 50 cycles, the capacity of both batteries decayed, with the stamped electrode battery maintaining 78.0% of its original capacity (109  $\text{mAh g}^{-1}$ ), whereas the capacity of the bar-coated electrode battery rapidly decayed to 50.6% (64  $\text{mAh g}^{-1}$ ). Figure 5b shows the stamped and bar-coated-T electrodes structural stability schematically. Considering the weak structural stability of the bar-coated electrode, the structure may collapse, causing the capacity decrease. We repeated the EIS measurements after the cycling tests to

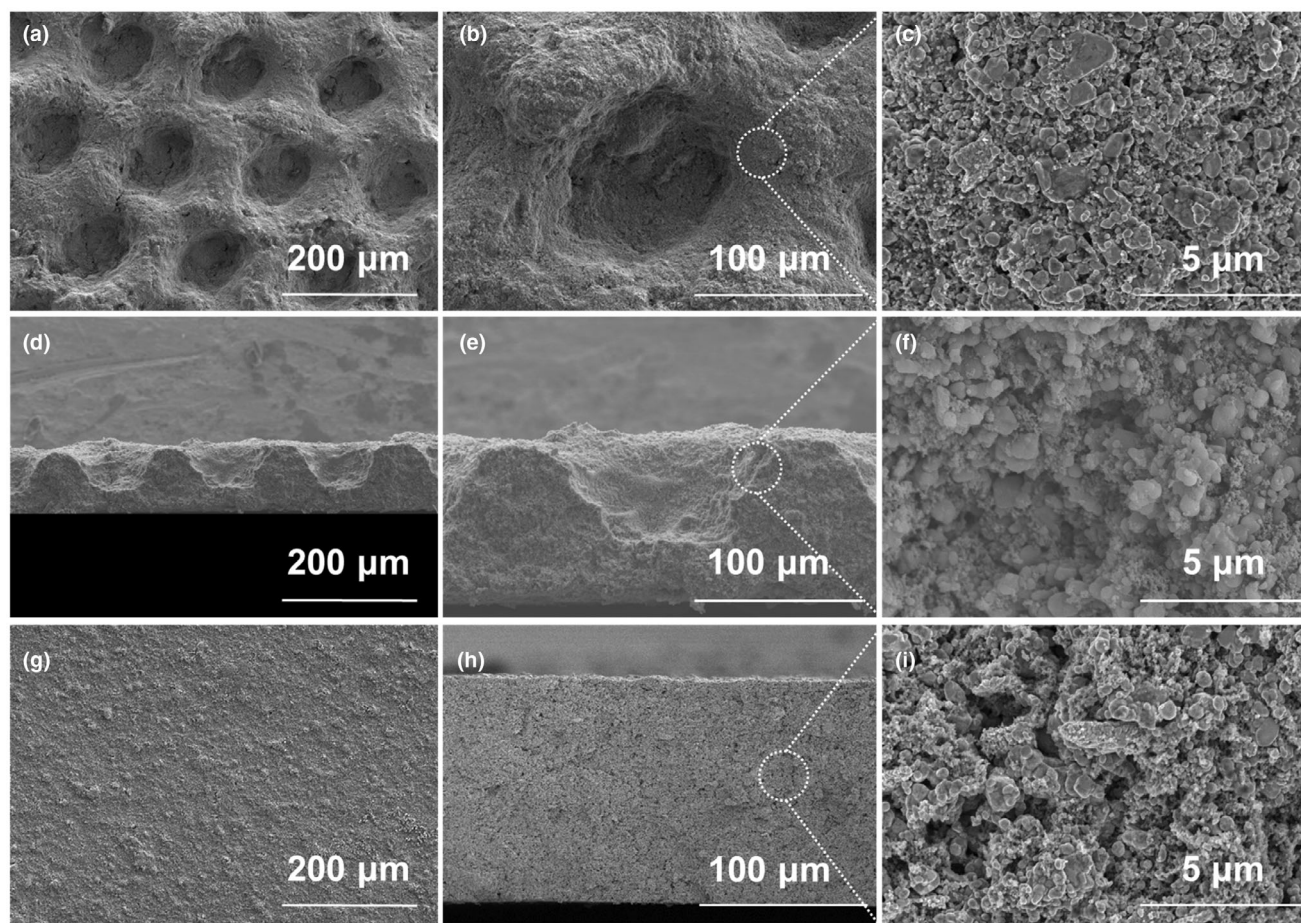


**Figure 3.** SEM images of the stamped and bar-coated electrodes. a–c) Top-view of the stamped electrode. d–f) Cross-section of the stamped electrode. g) Top-view of the conventional bar-coated electrode. h) Cross-section of the conventional bar-coated electrode. i) High-magnification image of the conventional bar-coated electrode.

investigate the stability of the stamped electrode. As shown in Figure 5c, the Nyquist plot of the stamped electrode did not change significantly after the cycling, indicating excellent electrode cycle stability. In the case of the bar-coated-T electrode (Figure 5d), the intercept of the Nyquist curve with  $\text{Re}(Z)$  and the diameter of the semicircle increased after the cycling test. The results indicated decayed electrical connectivity of the bar-coated-T electrode, most likely due to the cracking and flaking of the electrode material, potentially leading to unstable contact between the electrode and current collector. To verify this hypothesis, following the long cycle test, the batteries were disassembled to investigate the changes in the electrode structure. The stamped electrode remained intact with no observable cracks or material loss (Figure 5e). In contrast, two cracks spanning the entire bar-coated-T electrode and some missing electrode material were observed, exposing the current collector underneath it. In addition to the cracks, we observed prominent protrusions across the electrode surface, as shown in Figure 5f. The top-view and cross-sectional images of the stamped electrode (Figure 5g,h) showed no collapse or cracking of the microchannels, confirming the excellent structural stability of the stamped low-tortuosity electrode during the cycling process. The bar-coated-T electrode

showed significant cracking after the long cycle testing (Figure 5i). The cross-sectional view (Figure 5j) showed that the electrode was interspersed with cracks and some material was detached from the current collector. The protrusions along the cracks in the bar-coated-T electrode, shown in Figure S10a,b, Supporting Information, can cause uneven ion distribution during the battery charge–discharge, which may result in battery short circuit affecting the battery safety. In addition, the electrode material that detached from the current collector could no longer participate in the charge–discharge process, resulting in a rapid capacity decrease.

### 3. Conclusion

In conclusion, a fast-charging and highly stable low-tortuosity electrode was fabricated using a one-step stamping process. The electrode was prepared using low-cost and environmentally friendly water as the solvent. The stamped electrode exhibited a high charge capacity of  $101 \text{ mAh g}^{-1}$  at a current rate of 3 C, while the bar-coated M electrode has  $54 \text{ mAh g}^{-1}$  at 3 C with the same areal mass loading of



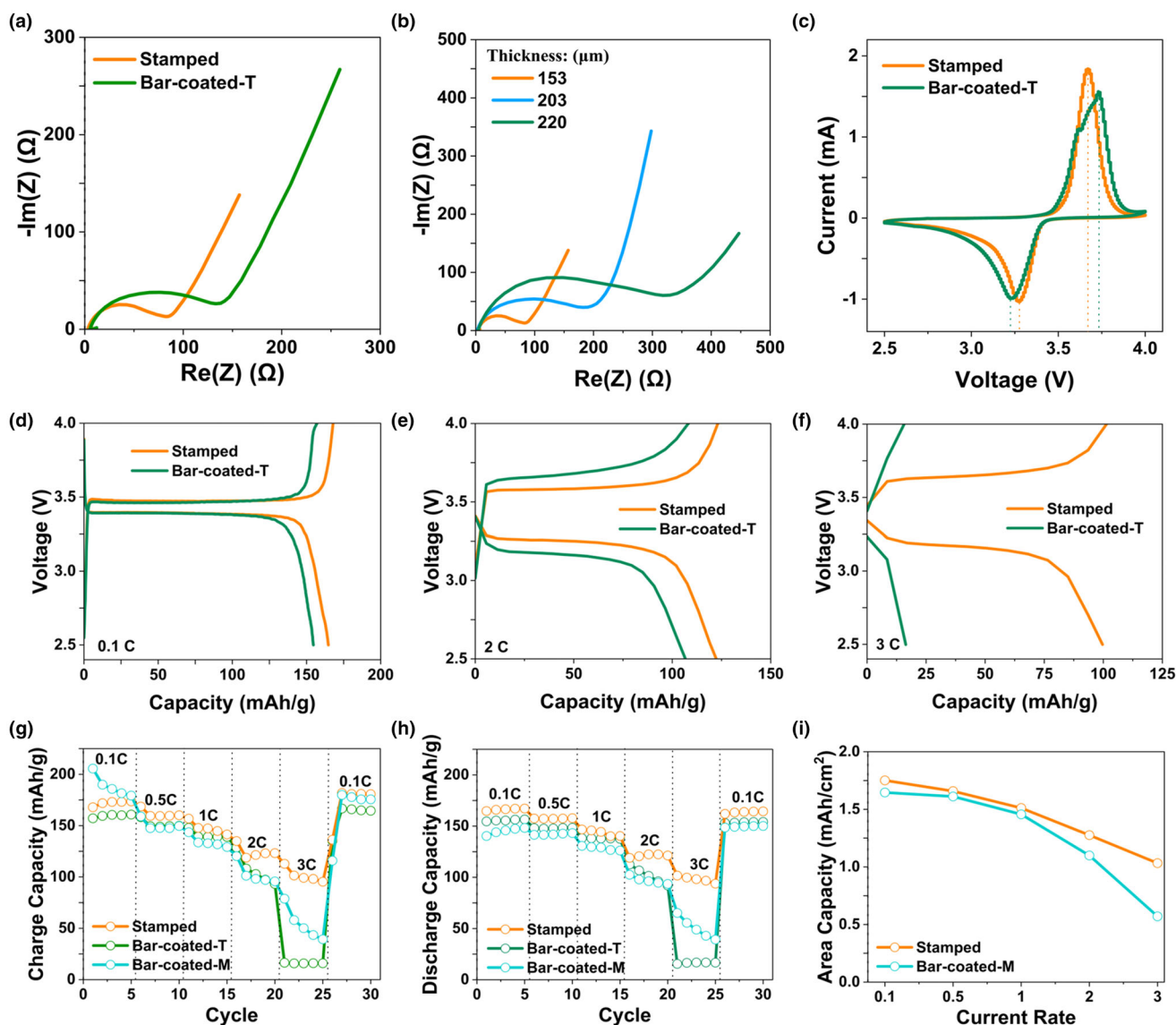


**Figure 4.** Electrochemical measurements of the cells fabricated using stamped and bar-coated-T electrodes. a) Nyquist plots of the stamped and bar-coated-T electrodes. b) Nyquist plots of stamped electrodes with different thicknesses. c) CV curves of the stamped and bar-coated-T electrodes at a scan rate of  $0.1 \text{ mV s}^{-1}$ . Galvanostatic charge and discharge profiles comparison for both cells at d) 0.1 C, e) 2 C, and f) 3 C. g, h) Rate performances of the stamped, bar-coated-T, and bar-coated-M electrodes at various rates from 0.1 to 3 C. i) Area capacities of the stamped and bar-coated-M electrodes at various rates from 0.1 to 3 C.

$\sim 11 \text{ mg cm}^{-2}$ , and the counterpart bar-coated T electrode has only  $16 \text{ mAh g}^{-1}$  at 3 C with the same thickness of  $\sim 155 \mu\text{m}$ . The EIS measurements revealed that the low-tortuosity electrode exhibited a lower resistance and better structural stability than the bar-coated electrode. Water and electrolyte contact angle characterization revealed that the low-tortuosity electrode exhibited a smaller water contact angle and faster electrolyte absorption rate than the bar-coated electrode. The stamped electrodes are straightforward and inexpensive to be fabricated and exhibited better fast-charging capability than the bar-coated electrodes. The scalability of the stamping technique makes it a promising industrial manufacturing process for low-tortuosity fast-charging

electrodes. This work provides innovative and feasible strategies for manufacturing fast-charging electrodes for practical applications in industry.

## 4. Experimental Section

Detailed information related to the synthesis of active electrodes, physicochemical characterization, and electrochemical evaluation of bifunctional electrodes towards UOR and supercapacitor application is provided in Supporting Information.

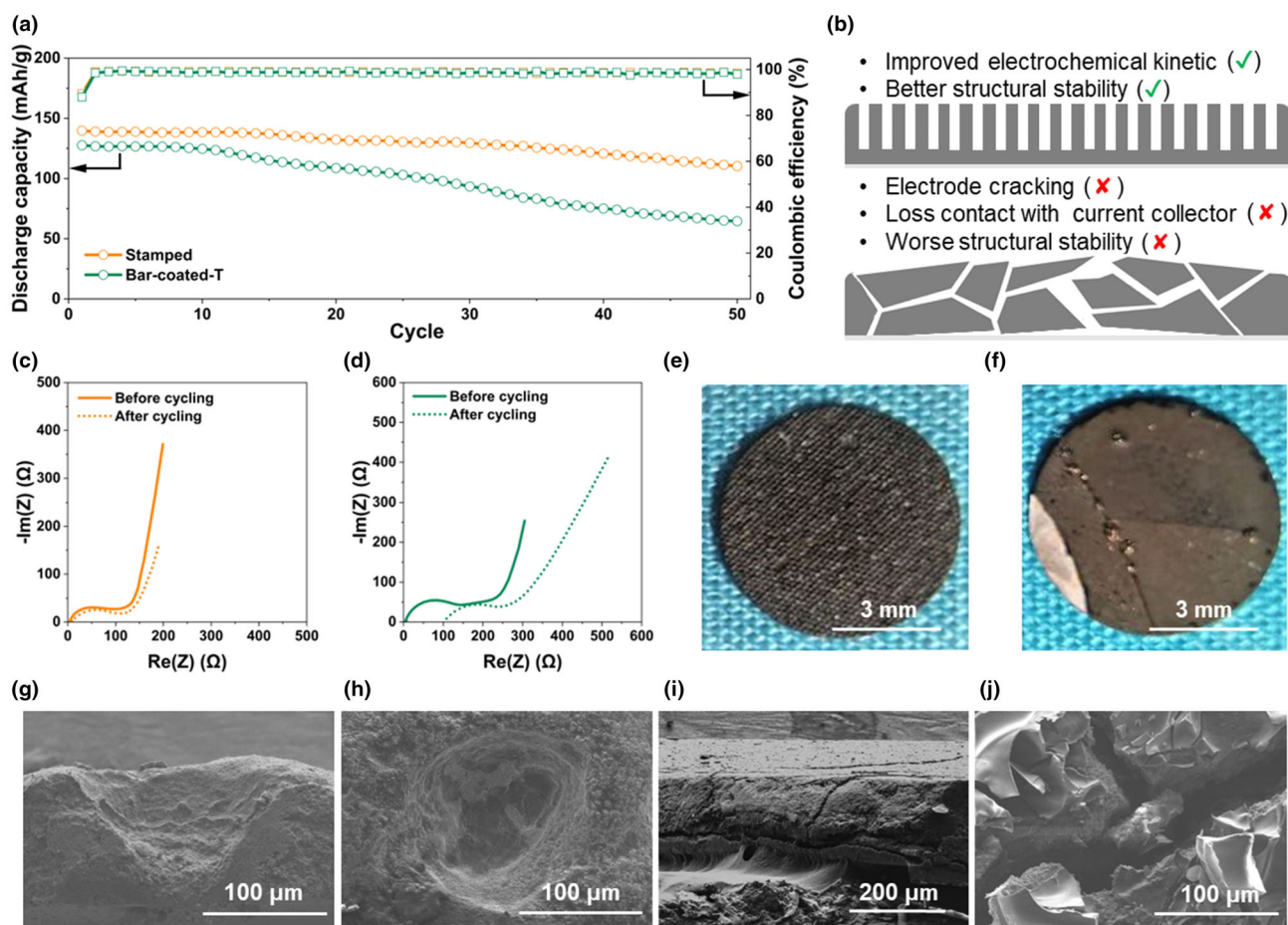


**Figure 5.** a) Cycling performance of the stamped and bar-coated-T electrodes at the rate of 1 C. b) Schematic representation of the stamped and bar-coated-T electrodes after the cycling test. c) Nyquist plots of the stamped electrode before and after the cycling test. d) Nyquist plots of the bar-coated-T electrode before and after the cycling test. e, f) Photographs of the stamped and bar-coated-T electrodes after the cycling test. g, h) Cross-section and top-view SEM images of the stamped electrode after the cycling test. i, j) Cross-section and top-view SEM images of the bar-coated electrode after the cycling test.

## Acknowledgements

H.Z. acknowledges the Advanced Manufacturing Office (award number DE-EE0009111) under Energy Efficiency and Renewable Energy (EERE) in United States Department of Energy. The author acknowledge the use of the Scanning Electron Microscope provided by the Boston Electron Microscopy Center at Northeastern University.

## Conflict of Interest

The authors declare no conflict of interest.

## Author Contributions

H.Z. conceived the study. H.R. conducted the primary experiments. H.Z. and H.R. wrote the article. Y.W. draw the schematics. D.C. revised the article. T.J. and X.S. conducted the SEM characterizations. W.G. polished the language. All authors discussed the results.

## Supporting Information

Supporting Information is available from the Wiley Online Library or from the author.

## Keywords

fast charging, kinetic, lithium-ion batteries, tortuosity, water solvent

Received: July 20, 2022

Revised: November 26, 2022

Published online: December 24, 2022

- [1] N. Nitta, F. Wu, J. T. Lee, G. Yushin, *Mater. Today* **2015**, *18*, 252.
- [2] A. J. Smith, J. C. Burns, J. R. Dahn, *Electrochem. Solid State Lett.* **2010**, *13*, A177.
- [3] Y. Wang, D. Cao, X. Sun, H. Ren, T. Ji, X. Jin, J. Morse, B. Stewart, H. Zhu, *Adv. Mater. Technol.* **2022b**, *7*, 2200303.
- [4] A. Tomaszewska, Z. Chu, X. Feng, S. O'Kane, X. Liu, J. Chen, C. Ji, E. Endler, R. Li, L. Liu, Y. Li, S. Zheng, S. Vetterlein, M. Gao, J. Du, M. Parkes, M. Ouyang, M. Marinescu, G. Offer, B. Wu, *eTransportation* **2019**, *1*, 100011.
- [5] Y. Liu, Y. Zhu, Y. Cui, *Nat. Energy* **2019**, *4*, 540.
- [6] C. Huang, M. Dontigny, K. Zaghib, P. S. Grant, *J. Mater. Chem. A* **2019**, *7*, 21421.
- [7] K. G. Gallagher, S. E. Trask, C. Bauer, T. Woehrle, S. F. Lux, M. Tschech, P. Lamp, B. J. Polzin, S. Ha, B. Long, Q. Wu, W. Lu, D. W. Dees, A. N. Jansen, *J. Electrochem. Soc.* **2015**, *163*, A138.

- [8] Y. Kuang, C. Chen, D. Kirsch, L. Hu, *Adv. Energy Mater.* **2019**, 9, 1901457.
- [9] E. R. Logan, J. R. Dahn, *Trends Chem.* **2020**, 2, 354.
- [10] J. Popovic, D. Hofler, J. P. Melchior, A. Munchinger, B. List, J. Maier, *J. Phys. Chem. Lett.* **2018**, 9, 5116.
- [11] G. Li, Z. Liu, Q. Huang, Y. Gao, M. Regula, D. Wang, L.-Q. Chen, D. Wang, *Nat. Energy* **2018**, 3, 1076.
- [12] C. Chen, Y. Zhang, Y. Li, Y. Kuang, J. Song, W. Luo, Y. Wang, Y. Yao, G. Pastel, J. Xie, L. Hu, *Adv. Energy Mater.* **2017**, 7, 1700595.
- [13] X. Gao, X. Liu, R. He, M. Wang, W. Xie, N. P. Brandon, B. Wu, H. Ling, S. Yang, *Energy Storage Mater.* **2021**, 36, 435.
- [14] X. Wang, T. Wang, J. Borovilas, X. He, S. Du, Y. Yang, *Nano Res.* **2019**, 12, 2002.
- [15] I. V. Thorat, D. E. Stephenson, N. A. Zacharias, K. Zaghbi, J. N. Harb, D. R. Wheeler, *J. Power Sources* **2009**, 188, 592.
- [16] J. S. Sander, R. M. Erb, L. Li, A. Gurijala, Y. M. Chiang, *Nat. Energy* **2016**, 1, 16099.
- [17] S. Wu, H. Zheng, X. Wang, N. Zhang, W. Cheng, B. Fu, H. Chen, H. Liu, H. Duan, *Chem. Eng. J.* **2022**, 430, 132810.
- [18] D. Cao, Y. Xing, K. Tantratian, X. Wang, Y. Ma, A. Mukhopadhyay, Z. Cheng, Q. Zhang, Y. Jiao, L. Chen, H. Zhu, *Adv. Mater.* **2019**, 31, e1807313.
- [19] L. L. Lu, Y. Y. Lu, Z. J. Xiao, T. W. Zhang, F. Zhou, T. Ma, Y. Ni, H. B. Yao, S. H. Yu, Y. Cui, *Adv. Mater.* **2018**, 30, e1706745.
- [20] T. Marks, S. Trussler, A. J. Smith, D. Xiong, J. R. Dahn, *J. Electrochem. Soc.* **2011**, 158, A51.
- [21] H. Zheng, L. Tan, G. Liu, X. Song, V. S. Battaglia, *J. Power Sources* **2012**, 208, 52.
- [22] Y. Wang, J. He, D. Cao, E. Cakmak, X. Zhao, Q. Wu, Y. Zhao, H. Ren, X. Sun, Y. Li, H. Zhu, *Energy Storage Mater.* **2023**, 55, 42.
- [23] L.-X. Yuan, Z.-H. Wang, W.-X. Zhang, X.-L. Hu, J.-T. Chen, Y.-H. Huang, J. B. Goodenough, *Energy Environ. Sci.* **2011**, 4, 269.
- [24] E. Bormashenko, *Adv. Colloid Interf. Sci.* **2015**, 222, 92.
- [25] K.-Y. Park, J.-W. Park, W. M. Seong, K. Yoon, T.-H. Hwang, K.-H. Ko, J.-H. Han, Y. Jaedong, K. Kang, *J. Power Sources* **2020**, 468, 228369.
- [26] Z. Chen, D. L. Danilov, L. H. J. Raijmakers, K. Chayambuka, M. Jiang, L. Zhou, J. Zhou, R.-A. Eichel, P. H. L. Notten, *J. Power Sources* **2021**, 509, 230345.